Roscam Abbing, Sylvianne D.C.; Kolkowski, Radoslaw; Zhang, Zhuang Yan; Campi, Filippo; Lötgering, Lars; Koenderink, A. Femius; Kraus, Peter M.

Extreme-Ultraviolet Shaping and Imaging by High-Harmonic Generation from Nanostructured Silica

Published in:
Physical Review Letters

DOI:
10.1103/PhysRevLett.128.223902

Published: 03/06/2022

Document Version
Publisher's PDF, also known as Version of record

Editors' Suggestion | Featured in Physics

Extreme-Ultraviolet Shaping and Imaging by High-Harmonic Generation from Nanostructured Silica

Sylvianne D. C. Roscam Abbing,[1,*] Radoslaw Kolkowski,[2,3] Zhuang-Yan Zhang,[1] Filippo Campi,[1] Lars Lötgering,[1] A. Femius Koenderink,[2] and Peter M. Kraus[1,4,†]

[1]*Advanced Research Center for Nanolithography (ARCNL), Science Park 106, 1098XG Amsterdam, Netherlands*
[2]*Center for Nanophotonics, AMOLF, Science Park 104, 1098XG Amsterdam, Netherlands*
[3]*Optics and Photonics Group, Department of Applied Physics, Aalto University, P.O. Box 13500, FI-00076 Aalto, Finland*
[4]*Department of Physics and Astronomy, and LaserLaB, Vrije Universiteit, De Boelelaan 1081, 1081HV Amsterdam, Netherlands*

(Received 23 December 2021; accepted 26 April 2022; published 31 May 2022)

Coherent extreme-ultraviolet pulses from high-harmonic generation have ample applications in attosecond science, lensless imaging, and industrial metrology. However, tailoring complex spatial amplitude, phase, and polarization properties of extreme-ultraviolet pulses is made nontrivial by the lack of efficient optical elements. Here, we have overcome this limitation through nanoengineered solid samples, which enable direct control over amplitude and phase patterns of nonlinearly generated extreme-ultraviolet pulses. We demonstrate experimental configurations and emitting structures that yield spatially patterned beam profiles, increased conversion efficiencies, and tailored polarization states. Furthermore, we use the emitted patterns to reconstruct height profiles, probe the near-field confinement in nanostructures below the diffraction limit of the fundamental radiation, and to image complex structures through coherent diffractive emission from these structures. Our results pave the way for introducing sub-fundamental-wavelength resolution imaging, direct manipulation of beams through nanoengineered samples, and metrology of nanostructures into the extreme-ultraviolet spectral range.

DOI: 10.1103/PhysRevLett.128.223902

Attosecond science and strong-field physics are undergoing a revolution through the recently discovered generation of high harmonics in solids [1–3]. Until now, high-harmonic generation (HHG) from dielectrics was shown to generate photon energies well into the extreme ultraviolet (XUV) photon energy range [4–6]. The flexibility associated with solid samples consequently promises achievements beyond those of gas-phase HHG [7], which enabled femto- and attosecond timescale [8–12] studies, and all-optical nanoscale XUV imaging [13,14]. All XUV experiments that rely on post-generation beam shaping are currently challenged by the lack of suitable optical elements: Refractive optics are limited by the high absorption of materials in the XUV and were only recently demonstrated by gas expansions with a spatially varying density profile close to a resonance [15]. Diffractive XUV focusing through binary amplitude shaping has recently been demonstrated for polychromatic HHG pulses [16]. However, binary diffraction elements are challenged by low efficiencies (10% for gratings [17]), whereas purely phase shifting elements would provide higher efficiencies (41% for gratings) but their realization is impractical due to the extremely short attenuation lengths in the XUV.

The possibility to nanostructure the emitting medium in solid HHG opens up the path towards tailored emission profiles, and to directly generate XUV patterns inside structures for imaging unknown objects through diffraction with sub-fundamental-wavelength resolution. First steps have been undertaken in HHG from engineered surfaces, albeit at relatively low photon energies and from larger structures [18–25]. In this report, we introduce and demonstrate XUV science of nanostructures by HHG. We show how the diffracted emission patterns can be quantitatively understood and modeled, and use this knowledge for first demonstrations to control the phase, amplitude, and polarization of the emitted XUV pulses at will. Moreover, we introduce XUV generation from complex structures and use the measured patterns to reconstruct the underlying nanoscale structures. Our results demonstrate profile retrieval in all three dimensions, paving the way towards imaging and semiconductor wafer metrology through solid-state HHG from structured materials.

To generate diffractive high harmonics in the XUV we focused 800 nm femtosecond pulses onto a grating-structured (10 μm pitch, 5 μm linewidth, 85 nm height) fused silica sample (112 ± 3 μm thick), as shown in Fig. 1(a). Only odd harmonics orders are observed, because fused

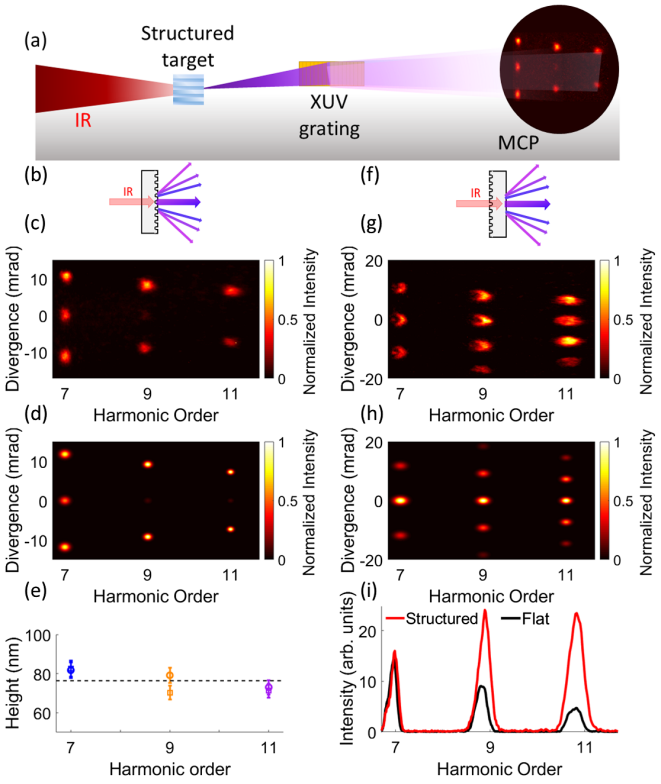

FIG. 1. (a) Experimental setup. (b),(c) Diffracted high harmonics generated inside the grating-structured rear surface. (d) Simulation of HHG diffraction from a near-field phase grating. (e) Height reconstruction, using the data from panel (c). (f),(g) Diffracted high harmonics generated by a phase-grating imprinted infrared pulse. (h) Simulation of HHG diffraction from a near-field amplitude grating. (i) Enhancement of HHG, total diffraction signal (red) compared to emission of a flat sample (black).

silica appears isotropic to HHG due to its small crystal-domain sizes. The absorption length in silica at the generated wavelengths is less than 20 nm [26], hence effective harmonic emission takes place only close to the interface between silica and vacuum at the rear surface, and phase matching over an extended volume of the emitted XUV is negligible. When the sample is oriented such that the flat surface faces the impinging pulses [Fig. 1(b)], harmonic orders 7 (H7), 9, and 11 are diffracted onto the detector [Fig. 1(c)]. At the structured rear surface, diffraction originates from a transverse phase modulation of the XUV emission, which is introduced by the optical path-length difference of the grating grooves, and therefore has a periodicity equal to the pitch of the grating. We simulated diffraction patterns [Fig. 1(d)] using an analytical model, assuming a phase grating in the near field (Supplemental Material [27]). The excellent agreement of photon-energy dependent diffraction angles and efficiencies between experiment and simulation confirms our model. The generation of HHG directly inside the diffractive grating-structured silica, which then entails a pure phase grating, leads to extremely efficient first-order diffraction. Specifically for H7, H9, and H11, the percentage of the sum of the signal diffracted into the first orders, compared to the sum of both the first and zeroth-order signals, is 70%, 90%, and 97%, respectively. We expect to also diffract light into the third orders and higher orders, but are unable to measure these orders in the present experimental configuration. The total measured diffracted signal is on the same order of magnitude as the total signal from a flat sample (Supplemental Material [27]). For H9 and H11 only little signal is diffracted into the zeroth order, which resembles the situation of the theoretical maximum of 41% diffraction efficiency in each first order [17]. The depth of the grooves of the grating can also be reconstructed from the measured wavelength-resolved diffraction efficiencies in Fig. 1(b). We employ an analytical model (Supplemental Material [27]) which allows to extract the modulation depth of a binary phase grating, and therefore the height of the grooves, with prior knowledge of only the refractive index of the bulk and the central wavelength, see Fig. 1(e). The three harmonic orders give an average height of 76 nm, which is close to the value of 85 nm measured with a profilometer. This demonstrates that HHG can be utilized as a tool for direct height metrology of a periodic sample through phase control of the XUV generation.

We now turn to a configuration where the sample is oriented such that the infrared pulses impinge on the structured surface first and harmonics are emitted from the rear flat surface [Fig. 1(f)]. The structured front surface imprints phase modulation onto the infrared beam, which translates into amplitude modulation on the flat rear surface, leading to diffraction patterns with the same emission angles, but markedly different intensity distributions [Fig. 1(g)] compared to the previous configuration [Figs. 1(b) and 1(c)]. Figure 1(h) shows a simulated spectrum, where we propagated the fundamental field to the rear surface by Fresnel diffraction, creating a modulated infrared intensity distribution (Supplemental Material [27]). HHG is effectively driven by a periodically modulated intensity distribution of the fundamental field, which facilitates the emission of both odd and even diffraction orders [Fig. 1(g), due to a limited field of view in the detection, we did not observe the even orders of H9 and H11 for positive divergence angles], whereas even diffraction orders are absent for the XUV phase grating with 50% duty cycle in Figs. 1(b)–1(d). In both configurations, the odd diffraction orders originate from modulations with a periodicity of 10 μm, the pitch of the grating. In addition, even diffraction orders appear as a cause of a modulation in the fundamental near field with a periodicity of 5 μm. We attribute this faster modulation due to the Fresnel propagation that repeats the initial phase grating after regular distances [35,36], the so-called Talbot length $z_T = 2na^2/\lambda$ (a is the pitch of the grating, n the refractive index). The thickness of our sample is on the same order of magnitude as half the Talbot length, such that the initial phase grating is repeated with a phase shift. This leads

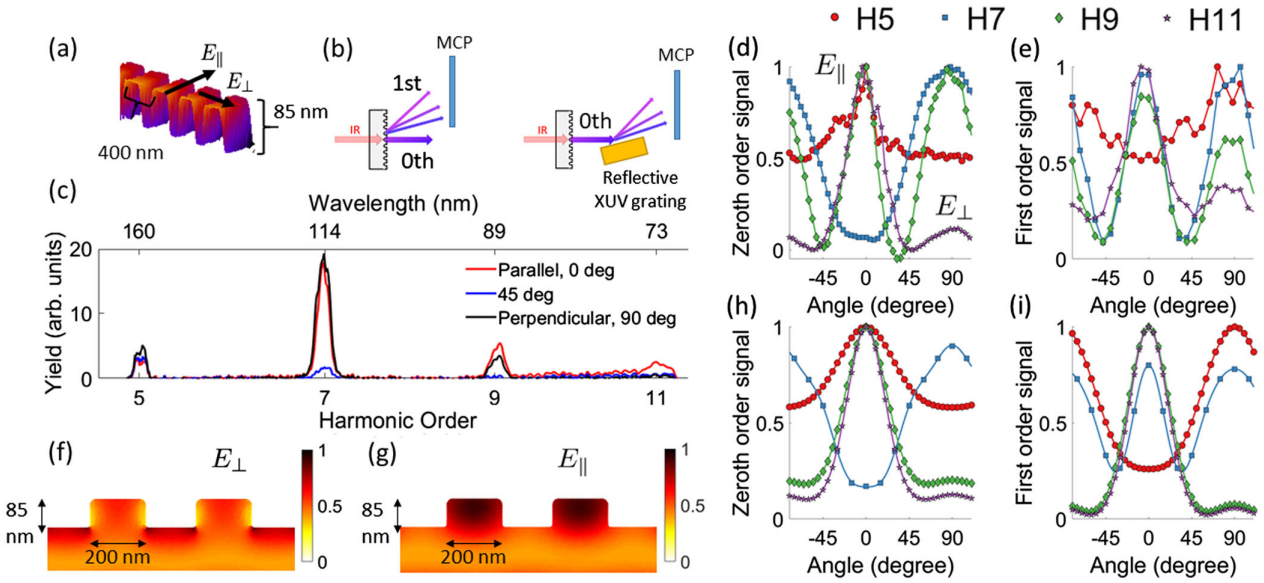

FIG. 2. (a) AFM image of the structure. (b) Schematic of setup, for detecting zeroth and first-order diffraction. (c) Polarization-dependent HHG. (d) Polarization-dependent zeroth-order diffraction. (e) Polarization-dependent first-order diffraction. (f),(g) Simulation of the near-field of 800 nm, when polarized perpendicular and parallel to the grooves, respectively. (h),(i) Simulated polarization-dependent zeroth and first-order diffraction signals.

to modulations in the fundamental intensity distribution in addition to the phase grating, causing the emission of even diffraction orders at the flat exit surface due to breaking of the original 50% duty cycle of the grating (Supplemental Material [27]). As before, experimental intensities and simulations [Fig. 1(h)] show good agreement. Additionally, the sinusoidal modulation of the amplitude imparted onto the fundamental field, determined by the geometric parameters of the grating structure and the sample thickness, gives rise to higher local power density, thus enhancing the conversion efficiency of light pulses at the fundamental frequency to HHG by about a factor of 2. Figure 1(i) shows a direct comparison between the divergence-integrated spectra generated in such configuration and spectra generated in a flat bulk material, with equal sample thickness. The enhancement is most pronounced for higher harmonic orders due to the nonlinear HHG process.

We have thus far shown the generation of structured XUV light and explained the underlying mechanism in periodic structures larger than the wavelength of the fundamental driving laser. We also demonstrated the ability to use the emitted harmonics to sense the amplitude distribution of the fundamental field at the generation interface and to reconstruct height profiles. We now turn to investigating light-matter interaction of intense femtosecond pulses with periodic structures with characteristic sizes smaller than the driving wavelength, in which the fundamental near field will be shaped by the geometry of the structure, which provides opportunities for controlling not only amplitude and phase, but also the polarization state of the emitted XUV light.

Generation inside a nanostructured fused-silica grating with sub-fundamental-wavelength dimensions [400 nm pitch, 200 nm linewidth, 85 nm height, Fig. 2(a)] is shown in Fig. 2. We observed first-order diffraction of the harmonics, when emission occurred on the structured side [Fig. 2(b)]. This demonstrates that also with these sub-fundamental-wavelength dimensions a phase grating can be imprinted onto the XUV wavefront, similar as in Fig. 1(b). The signal was absent when the structure was facing the incoming pulses, thus the mechanism of imprinting amplitude modulation on the fundamental wavefront [Fig. 1(f)] does not apply here, since the structural features are too small for the fundamental wavefront to diffract from. For 400-nm pulses, diffractive harmonic emission at both the flat and at the structured side is possible (Supplemental Material [27]). The diffractive XUV generation is caused not only by phase modification, but also by the near-field amplitude of the 800-nm pulses at the structured exit surface, which represents a powerful new control mechanism over XUV emission.

We demonstrate this by changing the near-field of the 800-nm pulses in the nanostructures at will by changing the polarization of the incoming pulses with respect to the grating grooves. We measured the polarization dependence of HHG through detecting both the first and zeroth-order diffracted harmonics, as shown in Fig. 2(b), left and right panel, respectively. The yield of the first diffraction orders [Fig. 2(c)] for three different polarization angles [0° (parallel with grooves), 45°, and 90° (perpendicular to grooves)] shows a significant dependence for each harmonic, demonstrating that the polarization indeed acts as a control parameter for XUV generation. In more detail, we observe that all harmonic intensities maximize at 0°, except for the zeroth-order of H7 and the first-order of H5, which minimize at this angle [see Figs. 2(d) and 2(e)]. The common features

among the polarization dependent intensities of the harmonics can be attributed to the effect of the sub-wavelength structure on the fundamental field distribution, which we simulated (Supplemental Material [27]) for parallel and perpendicular orientations, as shown in Figs. 2(f) and 2(g), respectively. For a perpendicular orientation the field is localized between the grooves, whereas for parallel orientation the field is concentrated inside the grooves. Consequently, the minimum signal for intermediate polarization angles around 45° in Figs. 2(d) and 2(e) arises from a less efficient generation of the harmonics, which is caused by the splitting of the fundamental field amplitude between the top and bottom grooves. Based on the near-field simulations in Figs. 2(f) and 2(g), we simulated the zeroth and first order diffracted harmonic signals, which are shown in Figs. 2(h) and 2(i). The simulations accurately capture the increased XUV generation at 0° and 90° and a minimum signal for intermediate polarization angles around 45°. A convergence study (Supplemental Material [27]) furthermore demonstrates fully converged simulations. Thus, we have shown that HHG can indeed be controlled by modifying the fundamental near-field distribution by changing the incoming polarization, and inversely this distribution can be probed using diffracted HHG.

Some intensity dependencies in Figs. 2(d) and 2(e) stand out and require deeper analysis: We observed a relatively weaker modulation of H5, which is below the band gap of silica and thus generated over a much longer interaction length than other harmonics. This leads to greater contributions from the unstructured bulk of the silica as compared to generation in the vicinity of the structured surface, thus reducing the overall intensity modulations as a function of angle between polarization and grooves, as reproduced by the simulations in Figs. 2(h) and 2(i). Another intensity dependence that requires further analysis is that of H7, which minimizes at 0°. H7 is just above the band gap of silica, so the cascaded frequency conversion steps and their interference may become relevant [28], as intermediate lower harmonics can be generated over the entire interaction length of the solid medium. We modeled H7 as interference between the direct upconversion of seven 800 nm photons, sum frequency generation of the fundamental and twice H3 for the first cascaded step, and H5 and twice the fundamental for the second cascade (Supplemental Material [27]), which reproduces the experimental data well. Inclusion of cascaded processes could possibly resolve discrepancies between experiments and simulations for other harmonics too, e.g., H9. Such a simulation would be challenged by the larger number of cascaded processes, and goes beyond the scope of our study, but may stimulate new theories.

The redistribution of field amplitudes along parallel and perpendicular components is reminiscent of a form birefringence of the nanostructured grating, which thus acts as a wave plate for the generated XUV pulses. The agreement between our simulations in Figs. 2(h) and 2(i) and experimental data in Figs. 2(d) and 2(e) lends confidence to ascribing polarization states to the emitted harmonics, which are extracted from the simulations. Table I summarizes the Stokes parameters of the zeroth and first diffraction order of all harmonics for the incident fundamental polarization angle of 45°. Different harmonics exhibit various degrees of elliptical polarization. For example, the zeroth-order of H5 is almost purely linearly polarized at 45° (Stokes parameter U), and intuitively expected as H5 is emitted over the unstructured bulk where no form birefringence occurs. On the other hand, the contribution of the circular polarization component (Stokes parameter V) exceeds 70% in the first order of H9 and H11. As the nonlinear susceptibility tensors for HHG in amorphous silica represents an isotropic medium, the elliptical polarization can only be attributed to structurally induced phase retardation between polarization components parallel and perpendicular with respect to the grating. These experiments and simulations have shown that HHG is sensitive to the geometry of the structure, and therefore can be used to investigate near-field effects. We foresee that using HHG to directly image the near-field distributions would allow us to further characterize the effects of strong field confinement [19,23], offering a new platform for ultrafast physics in nanostructured solids.

TABLE I. Polarization state of the zeroth and the first diffraction order for harmonic orders generated with 45° angle between polarization and grooves. The squared moduli of Stokes parameters Q, U, and V (corresponding to the contributions of linear 0°–90°, linear ±45°, and circular polarization states, respectively) are shown, normalized by the squared modulus of the I parameter (corresponding to the total field intensity).

Stokes parameters	Zeroth diffraction order				First diffraction order			
	H5	H7	H9	H11	H5	H7	H9	H11
$\lvert Q\rvert^2$	0.000	0.060	0.002	0.004	0.007	0.825	0.099	0.098
$\lvert U\rvert^2$	0.996	0.562	0.606	0.537	0.943	0.065	0.200	0.174
$\lvert V\rvert^2$	0.004	0.379	0.392	0.459	0.050	0.110	0.701	0.727

Here we take the first step in this direction and demonstrate direct imaging of periodic and aperiodic structures through harmonic emission. We chose a complex aperiodic structure ("smiley") patterned in silica by e-beam lithography shown in Fig. 3(a). We generated with 400 nm, for which the third harmonic dominates the diffracted signal. If HHG was more polychromatic, spectral filters would be needed to select a certain harmonic, or Fourier-transform imaging [14,37] could resolve the HHG spectrum pixel by pixel. The main beam is blocked out with a beam block, leading to the diffraction pattern of the smiley structure as shown in Fig. 3(b). The calculated diffraction pattern [Fig. 3(c)] matches well with the experimentally measured one, showing the same significant features of the diffraction pattern. In Fig. 3(d), the diffracted pattern is

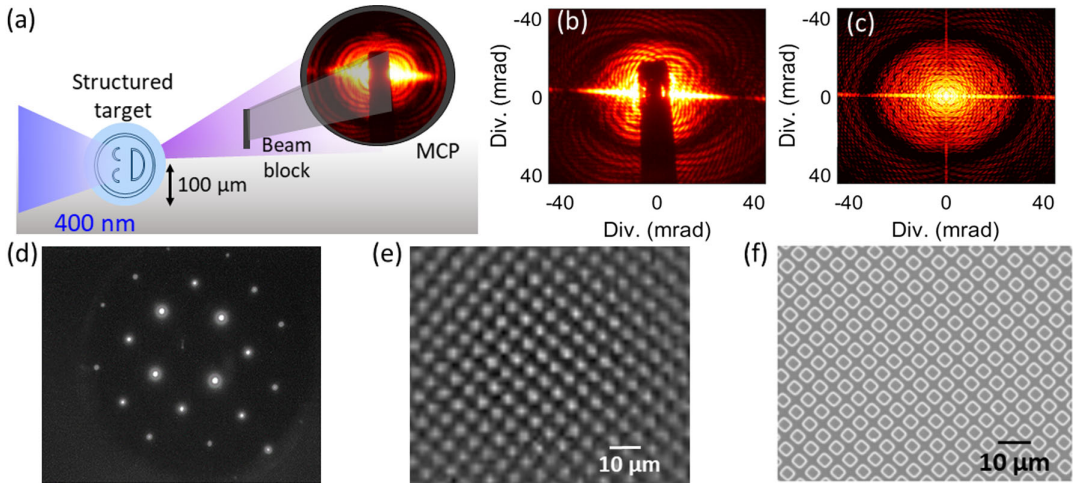

FIG. 3. (a) Schematic of experimental setup. (b) Measured diffraction pattern of target in (a). (c) Simulated diffraction pattern of target in (a). (d) Measured diffraction pattern of an array of micron-sized pillars. (e) Reconstructed surface. (f) Microscope image of the array of micron-sized pillars.

generated from an array of micron-sized pillars, with 2 μm dimensions, spaced four micrometers apart. In this particular diffraction pattern, the beam block will not block out any other diffraction signal, except the zeroth order, easing the reconstruction of the structure. The image reconstruction through a phase retrieval algorithm [38,39] in Fig. 3(e) correctly captures the orientation of the array, and the dimension as well as the spacing of the micron pillars. As a comparison, a microscope image of the pillar array is shown in Fig. 3(f). Compared to other HHG-based imaging techniques [40], here we can generate diffractive HHG directly from the structure of interest, which offers a new imaging tool for the inspection of patterned surfaces in the XUV.

The control of phase, amplitude, and polarization in solid HHG from nanostructures will allow sensing and even imaging femtosecond-resolved [41] electric near-field distributions in dielectric metasurfaces [19] and nanostructures. Moreover, the opportunity to shape XUV pulse properties at will opens new perspectives for pulse shaping that are otherwise challenging to achieve by modifications after generation. In particular, the demonstrated phase control can inspire the design of new highly efficient phase diffractive elements, such as zone plates, which will be more efficient than the typically used binary elements. This approach of combined generation and shaping in a single element may soon compete with postgeneration XUV shaping given the high efficiencies of XUV phase control [17] and the ongoing efforts to increase the efficiency of solid HHG [42,43].

Part of this work has been carried out at the Advanced Research Center for Nanolithography (ARCNL), a public-private partnership of the University of Amsterdam (UvA), the Vrije Universiteit Amsterdam (VU), the Dutch Research Council (NWO), and the semiconductor equipment manufacturer ASML, and was partly financed by Toeslag voor Topconsortia voor Kennis en Innovatie (TKI) from the Dutch Ministry of Economic Affairs and Climate Policy. We thank Reinout Jaarsma for technical support, and the mechanical workshop and the design, electronic, and software departments of ARCNL for support in constructing the setup. P. M. K. acknowledges support from NWO Veni Grant 016.Veni.192.254. Numerical simulations were performed at the research institute AMOLF, as part of the research programs Hybrid Nanophotonic Architectures for Ultrafast Quantum Optics (Project No. 680.47.621) and Nanophotonics for Solid-State Lighting (Project FOM-i33/680.93.33), both partly financed by NWO. Parts of the simulations were performed within the Aalto University School of Science Science-IT project, and were funded by the Academy of Finland Flagship Programme, Photonics Research and Innovation (PREIN), decision number: 320167.

*To whom all correspondence should be addressed. roscam@arcnl.nl
†To whom all correspondence should be addressed. kraus@arcnl.nl

[1] S. Ghimire, A. D. DiChiara, E. Sistrunk, P. Agostini, L. F. DiMauro, and D. A. Reis, Observation of high-order harmonic generation in a bulk crystal, Nat. Phys. **7**, 138 (2011).
[2] M. Hohenleutner, F. Langer, O. Schubert, M. Knorr, U. Huttner, S. Koch, M. Kira, and R. Huber, Real-time observation of interfering crystal electrons in high-harmonic generation, Nature (London) **523**, 572 (2015).
[3] O. Schubert, M. Hohenleutner, F. Langer, B. Urbanek, C. Lange, U. Huttner, D. Golde, T. Meier, M. Kira, S. W. Koch, and R. Huber, Sub-cycle control of terahertz high-harmonic generation by dynamical Bloch oscillations, Nat. Photonics **8**, 119 (2014).
[4] T. Luu, M. Garg, S. Y. Kruchinin, A. Moulet, M. T. Hassan, and E. Goulielmakis, Extreme ultraviolet high-harmonic spectroscopy of solids, Nature (London) **521**, 498 (2015).

[5] Y. S. You, Y. Yin, Y. Wu, A. Chew, X. Ren, F. Zhuang, S. Gholam-mirzaei, M. Chini, Z. Chang, and S. Ghimire, High-harmonic generation in amorphous solids, Nat. Commun. **8**, 724 (2017).

[6] T. T. Luu and H. J. Wörner, Measurement of the Berry curvature of solids using high-harmonic spectroscopy, Nat. Commun. **9**, 916 (2018).

[7] M. Ferray, A. L'Huillier, X. F. Li, L. A. Lompre, G. Mainfray, and C. Manus, Multiple-harmonic conversion of 1064 nm radiation in rare gases, J. Phys. B **21**, L31 (1988).

[8] P. M. Paul, E. S. Toma, P. Breger, G. Mullot, F. Augé, P. Balcou, H. G. Muller, and P. Agostini, Observation of a train of attosecond pulses from high harmonic generation, Science **292**, 1689 (2001).

[9] M. Hentschel, R. Kienberger, C. Spielmann, G. A. Reider, N. Milosevic, T. Brabec, P. Corkum, U. Heinzmann, M. Drescher, and F. Krausz, Attosecond metrology, Nature (London) **414**, 509 (2001).

[10] P. M. Kraus, B. Mignolet, D. Baykusheva, A. Rupenyan, L. Horny, E. F. Penka, G. Grassi, O. I. Tolstikhin, J. Schneider, F. Jensen, L. B. Madsen, A. D. Bandrauk, F. Remacle, and H. J. Wörner, Measurement and laser control of attosecond charge migration in ionized iodoacetylene, Science **350**, 790 (2015).

[11] P. M. Kraus, M. Zürch, S. K. Cushing, D. M. Neumark, and S. R. Leone, The ultrafast X-ray spectroscopic revolution in chemical dynamics, Nat. Rev. Chem. **2**, 82 (2018).

[12] P. M. Kraus and H. J. Wörner, Perspectives of attosecond spectroscopy for the understanding of fundamental electron correlations, Angew. Chem. Int. Ed. **57**, 5228 (2018).

[13] R. L. Sandberg, A. Paul, D. A. Raymondson, S. Hädrich, D. M. Gaudiosi, J. Holtsnider, R. I. Tobey, O. Cohen, M. M. Murnane, H. C. Kapteyn, C. Song, J. Miao, Y. Liu, and F. Salmassi, Lensless Diffractive Imaging using Tabletop Coherent High-Harmonic Soft-X-ray Beams, Phys. Rev. Lett. **99**, 098103 (2007).

[14] S. Witte, V. T. Tenner, D. W. Noom, and K. S. Eikema, Lensless diffractive imaging with ultra-broadband table-top sources: From infrared to extreme-ultraviolet wavelengths, Light Sci. Appl. **3**, e163 (2014).

[15] L. Drescher, O. Kornilov, T. Witting, G. Reitsma, N. Monserud, A. Rouzée, J. Mikosch, M. J. Vrakking, and B. Schütte, Extreme-ultraviolet refractive optics, Nature (London) **564**, 91 (2018).

[16] L. Loetgering, X. Liu, A. C. De Beurs, M. Du, G. Kuijper, K. S. Eikema, and S. Witte, Tailoring spatial entropy in extreme ultraviolet focused beams for multispectral ptychography, Optica **8**, 130 (2021).

[17] D. Paganin *et al.*, *Coherent X-ray optics* (Oxford University Press Demand, New York, 2006), Chap. 3.

[18] M. Sivis, M. Taucer, G. Vampa, K. Johnston, A. Staudte, A. Y. Naumov, D. Villeneuve, C. Ropers, and P. Corkum, Tailored semiconductors for high-harmonic optoelectronics, Science **357**, 303 (2017).

[19] H. Liu, C. Guo, G. Vampa, J. L. Zhang, T. Sarmiento, M. Xiao, P. H. Bucksbaum, J. Vučković, S. Fan, and D. A. Reis, Enhanced high-harmonic generation from an all-dielectric metasurface, Nat. Phys. **14**, 1006 (2018).

[20] G. Vampa, B. Ghamsari, S. S. Mousavi, T. Hammond, A. Olivieri, E. Lisicka-Skrek, A. Y. Naumov, D. Villeneuve, A. Staudte, P. Berini, and P. B. Corkum, Plasmon-enhanced high-harmonic generation from silicon, Nat. Phys. **13**, 659 (2017).

[21] K. Imasaka, T. Kaji, T. Shimura, and S. Ashihara, Antenna-enhanced high harmonic generation in a wide-bandgap semiconductor ZnO, Opt. Express **26**, 21364 (2018).

[22] S. Han, H. Kim, Y. W. Kim, Y.-J. Kim, S. Kim, I.-Y. Park, and S.-W. Kim, High-harmonic generation by field enhanced femtosecond pulses in metal-sapphire nanostructure, Nat. Commun. **7**, 13105 (2016).

[23] D. Franz, S. Kaassamani, D. Gauthier, R. Nicolas, M. Kholodtsova, L. Douillard, J.-T. Gomes, L. Lavoute, D. Gaponov, N. Ducros *et al.*, All semiconductor enhanced high-harmonic generation from a single nanostructured cone, Sci. Rep. **9**, 5663 (2019).

[24] A. Korobenko, S. Rashid, C. Heide, A. Y. Naumov, D. A. Reis, P. Berini, P. B. Corkum, and G. Vampa, Generation of structured coherent extreme ultraviolet beams from an MgO crystal, Opt. Express **29**, 24161 (2021).

[25] M. R. Shcherbakov, H. Zhang, M. Tripepi, G. Sartorello, N. Talisa, A. AlShafey, Z. Fan, J. Twardowski, L. A. Krivitsky, A. I. Kuznetsov *et al.*, Generation of even and odd high harmonics in resonant metasurfaces using single and multiple ultra-intense laser pulses, Nat. Commun. **12**, 4185 (2021).

[26] L. V. Rodríguez-de Marcos, J. I. Larruquert, J. A. Méndez, and J. A. Aznárez, Self-consistent optical constants of SiO_2 and Ta_2O_5 films, Opt. Mater. Express **6**, 3622 (2016).

[27] See Supplemental Material at http://link.aps.org/supplemental/10.1103/PhysRevLett.128.223902 for details on sample fabrication (I), experimental setup (II), experimental results and data analysis (III), and simulations of HHG from nanostructures (IV), which includes Refs. [4,26,28–34].

[28] O. Doron, L. Michaeli, and T. Ellenbogen, Direct and cascaded collective third-harmonic generation in metasurfaces, J. Opt. Soc. Am. B **36**, E71 (2019).

[29] S. Roscam Abbing, F. Campi, F. Sajjadian, N. Lin, P. Smorenburg, and P. M. Kraus, Divergence Control of High-Harmonic Generation, Phys. Rev. Applied **13**, 054029 (2020).

[30] S. D. C. Roscam Abbing, F. Campi, A. Zeltsi, P. Smorenburg, and P. M. Kraus, Divergence and efficiency optimization in polarization-controlled two-color high-harmonic generation, Sci. Rep. **11**, 24253 (2021).

[31] D. C. O'Shea, T. J. Suleski, A. D. Kathman, and D. W. Prather, *Diffractive Optics: Design, Fabrication, and Test* (SPIE Press, Bellingham, 2004), Vol. 62, pp. 83–85.

[32] G. Bachelier, J. Butet, I. Russier-Antoine, C. Jonin, E. Benichou, and P.-F. Brevet, Origin of optical second-harmonic generation in spherical gold nanoparticles: Local surface and nonlocal bulk contributions, Phys. Rev. B **82**, 235403 (2010).

[33] R. Kolkowski, L. Petti, M. Rippa, C. Lafargue, and J. Zyss, Octupolar plasmonic meta-molecules for nonlinear chiral watermarking at subwavelength scale, ACS Photonics **2**, 899 (2015).

[34] R. Kolkowski and A. F. Koenderink, Gain-induced scattering anomalies of diffractive metasurfaces, Nanophotonics **9**, 4273 (2020).

[35] H. F. Talbot, LXXVI. facts relating to optical science. no. IV, London, Edinburgh Dublin Philos. Mag. J. Sci. **9**, 401 (1836).

[36] L. Rayleigh, XXV. on copying diffraction-gratings, and on some phenomena connected therewith, London, Edinburgh Dublin Philos. Mag. J. Sci. **11**, 196 (1881).

[37] G. Jansen, D. Rudolf, L. Freisem, K. Eikema, and S. Witte, Spatially resolved Fourier transform spectroscopy in the extreme ultraviolet, Optica **3**, 1122 (2016).

[38] J. Miao, P. Charalambous, J. Kirz, and D. Sayre, Extending the methodology of X-ray crystallography to allow imaging of micrometre-sized non-crystalline specimens, Nature (London) **400**, 342 (1999).

[39] T. Latychevskaia, Iterative phase retrieval in coherent diffractive imaging: Practical issues, Appl. Opt. **57**, 7187 (2018).

[40] D. F. Gardner, M. Tanksalvala, E. R. Shanblatt, X. Zhang, B. R. Galloway, C. L. Porter, R. Karl Jr, C. Bevis, D. E. Adams, H. C. Kapteyn *et al.*, Subwavelength coherent imaging of periodic samples using a 13.5 nm tabletop high-harmonic light source, Nat. Photonics **11**, 259 (2017).

[41] Z. Wang, H. Park, Y. H. Lai, J. Xu, C. I. Blaga, F. Yang, P. Agostini, and L. F. DiMauro, The roles of photo-carrier doping and driving wavelength in high harmonic generation from a semiconductor, Nat. Commun. **8**, 1686 (2017).

[42] T. T. Luu, V. A. S. Cagnoli, S. U. Saha, and L. J. H. Eyderman, Generation of coherent extreme ultraviolet radiation from α-quartz using 50 fs laser pulses at a 1030 nm wavelength and high repetition rates, Opt. Lett. **43**, 1790 (2018).

[43] F. Campi, S. D. C. Roscam Abbing, Z.-Y. Zhang, M. van der Geest, and P. M. Kraus, Efficient extreme-ultraviolet multi-band high-order wave mixing in silica, in *International Conference on X-Ray Lasers 2020* (International Society for Optics and Photonics, 2021), Vol. 11886, p. 118860G, 10.1117/12.2593359.